JOC Article

$^{13}C-^{1}H$ and $^{13}C-^{13}C$ NMR *J*-Couplings in ^{13}C-Labeled *N*-Acetyl-neuraminic Acid: Correlations with Molecular Structure

Thomas Klepach,[†] Wenhui Zhang,[†] Ian Carmichael,[‡] and Anthony S. Serianni*,[†]

Department of Chemistry and Biochemistry, and the Radiation Laboratory, University of Notre Dame, Notre Dame, Indiana 46556-5670

aseriann@nd.edu

Received October 10, 2007

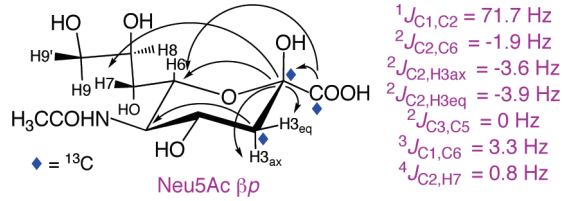

N-Acetyl-neuraminic acid (Neu5Ac, **2**) was prepared enzymatically containing single sites of ^{13}C-enrichment at C1, C2, and C3. Aqueous solutions of the three ^{13}C isotopomers were studied by ^{1}H and ^{13}C NMR spectroscopy at p^{2}H 2 and pH 8 to obtain J_{CH} and J_{CC} values involving the labeled carbons. Experimental studies were complemented by DFT calculations of the same set of *J*-couplings in protonated and ionized structural mimics of **2** to determine how well theoretical predictions match the experimental findings in saccharides bearing ionizable functionality. Results show that: (a) $^{2}J_{C2,H3ax/eq}$ values in **2** depend on anomeric configuration, thus complementing $^{3}J_{C1,H3ax/eq}$ behavior, (b) J_{CH} and J_{CC} values involving C2 depend on anomeric configuration, the C1−C2 bond torsion, and solution pH, and (c) long-range $^{4}J_{C2,H7}$ is sensitive to glycerol side-chain conformation. Intraring J_{HH} and most $^{2}J_{CH}$, $^{3}J_{CH}$, $^{2}J_{CC}$, and $^{3}J_{CC}$ involving C1−C3 of **2** appear largely unaffected by the ionization state of the carboxyl group. *In vacuo* and solvated DFT calculations of geminal and vicinal J_{CH} and J_{CC} values are similar and reproduce the experimental data well, but better agreement with experiment was observed for $^{1}J_{C1,C2}$ in the solvated calculations. The present work provides new information for future treatments of trans-glycoside couplings involving Neu5Ac residues by (a) providing new standard values of intraring J_{CC} for coupling pathways that mimic those for trans-glycoside J_{CC}, (b) identifying potential effects of solution pH on trans-glycoside couplings inferred through the behavior of related intraring couplings, and (c) providing specific guidelines for more reliable DFT predictions of J_{CH} and J_{CC} values in ionizable saccharides.

Introduction

Mammalian glycobiology can be distinguished from the glycobiology of other organisms based on the involvement of two monosaccharide building blocks, L-fucose (6-deoxy-L-galactose, Fuc) (**1**) and *N*-acetyl-neuraminic acid (NANA, Neu5Ac, sialic acid, SA) (**2**). Glycoproteins such as human IgG[1] contain **1** in the α-pyranosyl form (**1**α*p*), whereas the biological glycosyl donor, GDP-L-fucose (**3**), contains **1** in the *β*-configuration. The α-ketoacid, Neu5Ac, is also incorporated into glycoproteins in its α-pyranose configuration (**2**α*p*), and like **3**, the corresponding biological glycosyl donor, CMP-sialic acid

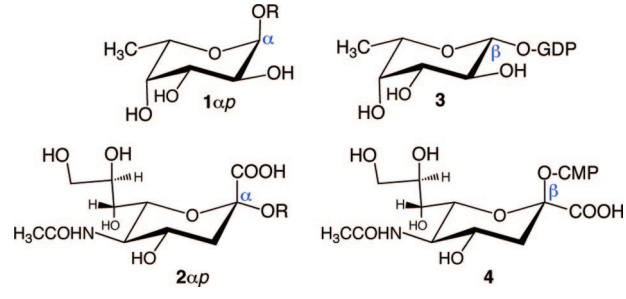

(**4**), contains **2** in the *β*-configuration. Incorporation of both monosaccharides into a growing oligosaccharide chain, catalyzed

[†] Department of Chemistry and Biochemistry.
[‡] Radiation Laboratory.

(1) Fujii, S.; Nishiura, T.; Nishikawa, A.; Miura, R.; Taniguchi, N. *J. Biol. Chem.* **1990**, *265*, 6009–6018.

(2) Wormald, M. R.; Rudd, P. M.; Harvey, D. J.; Chang, S.-C.; Scragg, I. G.; Dwek, R. A. *Biochemistry* **1997**, *36*, 1370–1380.

10.1021/jo702204x CCC: $40.75
Published on Web 05/20/2008

by appropriate glycosyltransferases, involves inversion of configuration at the anomeric center of both donor sugars.[2–4]

Neu5Ac residues are important in human biology and pathology. These residues are commonly found as terminal residues on N-linked oligosaccharide chains of glycoproteins or glycolipids and are accessible for binding to various biological agents. For example, Neu5Ac residues found on the outer lining of the stomach cavity during inflammation serve as binding sites for *Helicobacter pylori*, the causative agent of peptic ulcers.[5] The H5N1 virus associated with the avian flu is released from its host cell membrane through the action of a viral neuraminidase (sialidase), which cleaves the cell surface viral Neu5Ac receptor.[6] The antiviral agent, oseltamivir (Tamiflu), inhibits this enzyme, thus preventing the release of viral progeny and stifling the proliferation of the disease.[6,7] Removal of terminal Neu5Ac residues from human glycoproteins such as IgG targets the protein for clearance and degradation.[8]

Neu5Ac in *N*-glycans of human glycoproteins is commonly found linked glycosidically to β-D-Gal*p* in either α-(2→3) (**5**) or α-(2→6) (**6**) linkages (Scheme 1). The conformational properties of these linkages in solution remain poorly characterized, partly because only one $^3J_{COCH}$ coupling exists across them (Scheme 1) (this also pertains to linkages involving 2-ketosugars), in contrast to two $^3J_{COCH}$ across linkages involving aldopyranosyl rings. The common ^{1}H−^{1}H NOE in oligosaccharides between protons appended to the linkage carbons is also absent. However, useful structural information is potentially available from the five trans-glycoside (inter-residue) J_{CC} values across Neu5Ac glycosidic linkages (Scheme 1). A prerequisite to the use of these couplings as potential probes of linkage conformation is knowledge of their structural dependencies, and a first step toward achieving this aim is an understanding of J_{CC} values within Neu5Ac itself. For example, the intraring *J*-coupling between C1 and C6 and the trans-glycoside *J*-coupling between C1 and C3′ in **5** involve similar coupling pathways. Likewise, intraring coupling between C2 and C7 in **5** is similar to the trans-glycoside *J*-coupling between C2 and C2′/C4′ (Scheme 1).

Free Neu5Ac exists in aqueous solution in five monomeric forms: α- (**2**α*p*) and β- (**2**β*p*) pyranoses, keto (**2***k*), keto hydrate (**2***h*), and enol (**2***e*) (Scheme S1).[9] The β-pyranose **2**β*p* is highly predominant (∼91%), followed by **2**α*p* (∼6%). In the present work, three Neu5Ac isotopomers containing selective ^{13}C-labeling at C1, C2, and C3 (denoted **2**^{1}, **2**^{2}, and **2**^{3}, respectively; Scheme 2) were employed to permit measurements of intraring

SCHEME 1. α-(2→3) and α(2→3) Glycosidic Linkages Involving 2 and *trans*-Glycoside *J*-Couplings Across an α(2→3) Linkage

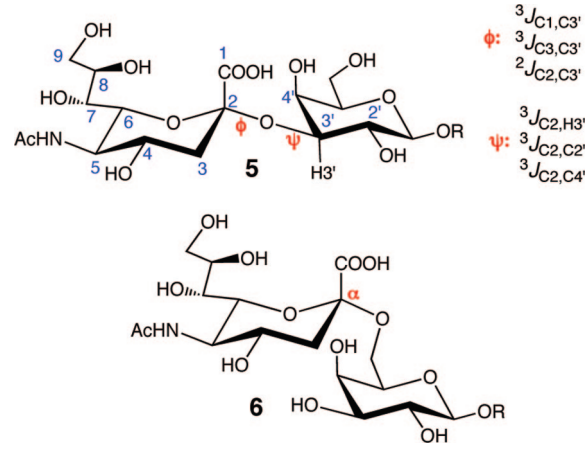

SCHEME 2. ^{13}C Isotopomers of 2 and Atom Numbering

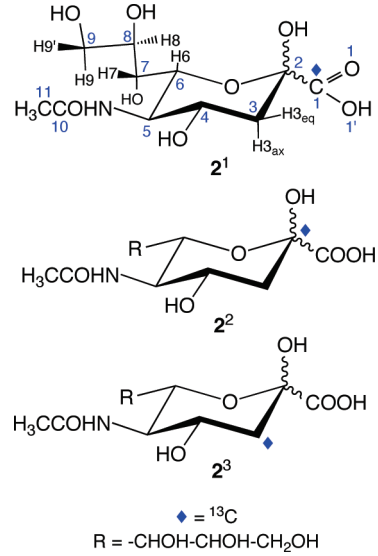

J_{CH} and J_{CC} values in aqueous solution involving the labeled carbons of **2**α*p* and **2**β*p*. Since ionization state may influence these couplings, measurements were conducted at p^{2}H 2.0 and pH 8.0 where the carboxyl group is largely protonated and deprotonated, respectively. Experimental studies were complemented by density functional theory (DFT) calculations of J_{CH} and J_{CC} in structural mimics in protonated and ionized states. Since the experimental ^{13}C−^{1}H and ^{13}C−^{13}C *J*-couplings in **2** pertain to conformationally rigid pathways, they can be compared to corresponding theoretical couplings to determine the accuracy of the latter when calculated in a saccharide capable of ionization. This type of comparison has not been reported previously and contributes to the long-term goal of interpreting trans-glycoside J_{CH} and J_{CC} across Neu5Ac glycosidic linkages where conformational flexibility is possible and reliance on theoretical calculations to predict their magnitudes is essential.

Experimental Methods

A. ^{13}C-Labeled *N*-Acetyl-neuraminic Acid (2^1, 2^2, and 2^3). Compounds **2**$^{1-3}$ were obtained from a commercial supplier and were used without further purification.

B. NMR Spectroscopy. For solutions at p^{2}H 2.0 or 8.0, solid samples of **2**^{1}, **2**^{2}, or **2**^{3} (free acid) were dissolved in ^{2}H$_2$O, and the

(3) Masuda, K.; Yamaguchi, Y.; Kato, K.; Takahashi, N.; Shimada, I.; Arata, Y. *FEBS* **2000**, *473*, 349–357.

(4) (a) Breton, C.; Snajdrova, L.; Jeanneau, C.; Koca, J.; Imberty, A. *Glycobiology* **2006**, *16*, 29R–37R. (b) Lairson, L. L.; Wakarchuk, W. W.; Withers, S. G. *Chem. Commun.* **2007**, *365*, 367.

(5) Mahdavi, J.; Sondén, B.; Hurtig, M.; Olfat, F. O.; Forsberg, L.; Roche, N.; Ångstrom, J.; Larsson, T.; Teneberg, S.; Karlsson, K.-A.; Altraja, S.; Wadström, T.; Kersulyte, D.; Berg, D. E.; Dubois, A.; Petersson, C.; Magnusson, K-E.; Norberg, T.; Lindh, F.; Lundskog, B. B.; Arnqvist, A.; Hammarström, L.; Borén, T. *Science* **2002**, *297*, 573–578.

(6) (a) Russell, R. J.; Haire, L. F.; Stevens, D. J.; Collins, P. J.; Lin, Y. P.; Blackburn, G. M.; Hay, A. J.; Gamblin, S. J.; Skehel, J. J. *Nature* **2006**, *443*, 45–49. (b) Rameix Welti, M. A.; Agou, F.; Buchy, P.; Mardy, S.; Aubin, J. T.; Veron, M.; van der Werf, S.; Naffakh, N. *Antimicrob. Agents Chemother.* **2006**, *50*, 3809–3815.

(7) (a) Palese, P.; Ueda, M.; Tobita, K.; Compans, R. W. *Virology* **1974**, *61*, 397–410. (b) Kim, C. U.; Williams, M. A.; Lui, H.; Zhang, L.; Swaminathan, S.; Bischofberger, N.; Chen, M. S.; Mendel, D. B.; Tai, C. Y.; Laver, W. G.; Stevens, R. C. *J. Am. Chem. Soc.* **1997**, *119*, 681–690.

(8) Morell, A. G.; Gregoriadis, G.; Scheinberg, H.; Hickman, J.; Ashwell, G. *J. Biol. Chem.* **1971**, *246*, 1461–1467.

(9) Klepach, T.; Carmichael, I.; Serianni, A. S. *J. Am. Chem. Soc.* **2008**, in press.

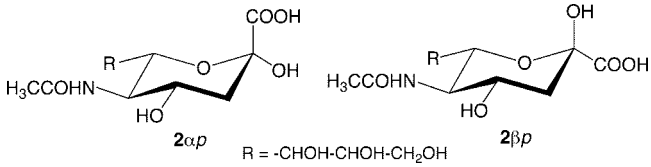

solution p^2H was adjusted to 2.0 or 8.0 using NaO^2H. For solutions at pH 2.0 or 8.0, solid samples were dissolved in distilled water and adjusted to pH 2.0 or 8.0 with NaOH. Sample concentrations were ~100 mM for ^1H and ~300 mM for ^{13}C NMR analyses.

High-resolution ^1H and $^{13}C\{^1H\}$ NMR spectra were collected at 600 and 150 MHz, respectively, at ~25 °C in 3 mm NMR tubes using a 3 mm $^{13}C/^1H$ microprobe (Nalorac). Digital resolutions for ^1H and $^{13}C\{^1H\}$ spectra were typically <0.02 Hz/pt and <0.1 Hz/pt, respectively. Spectra were processed with different degrees of resolution enhancement to improve the detection and measurement of smaller J_{HH}, J_{CH}, and J_{CC} values.

Calculational Methods

Model structures **7**−**10** were chosen for theoretical studies of J_{HH}, J_{CH}, and J_{CC}. These structures mimic the protonated and ionized forms of **2** in the α-(**7**/**8**) and β-pyranose (**9**/**10**) forms and in the $^2C_5$ ring conformation. Geometric optimization was performed in *Gaussian*03[10] using density functional theory (DFT) with the B3LYP functional[11] and the 6-31G* basis set[12] as described previously.[13,14a]

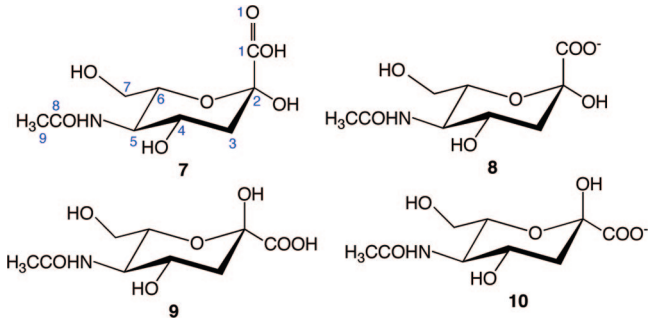

Four series of calculations were conducted to give a total of 16 data sets (four per structure). In all sets, the O1−C1−C2−O6 torsion angle (see structure **7** for atom numbering) was varied in 30° increments through 360°. In all sets, the C6−C7−O7−H and H4−C4−O4−H torsion angles were fixed at 180°; the O6−C6−C7−O7 torsion angle was fixed at 60°; and the H5−C5−N5−H and C5−N5−C8−C9 torsion angles were set initially at 180° and allowed to optimize (Scheme S2). The C3−C2−O2−H torsion was fixed at 180° in series 1 and 3, whereas it was set initially at 180° and allowed to optimize in series 2 and 4. Series 1/2 and 3/4 were otherwise identical except that the former pair involved *in vacuo* calculations, whereas the latter pair included the effects of solvent–water (see below). Data from each series are distinguished throughout the manuscript with the following symbolism, illustrated here for structure **7**: $\mathbf{7}^{FX}$ (series 1), $\mathbf{7}^{FL}$ (series 2), $\mathbf{7}^{FXS}$ (series 3), and $\mathbf{7}^{FLS}$ (series 4).

TABLE 1. $^1H-^1H$ Spin-Coupling Constants[a] in 2 at p^2H 2.0 and pH 8.0

	2α*p*		2β*p*	
J-coupling (Hz)	p^2H 2.0	pH 8.0	p^2H 2.0	pH 8.0
$^3J_{H3ax,\ H4}$	11.4	11.4	11.4	11.5
$^3J_{H3eq,H4}$	4.6	~4.1	4.9	4.9
$^2J_{H3ax,H3eq}$	−12.8	−12.5	−13.1	−13.0
$^3J_{H4,H5}$	obsc	obsc	10.1	9.9
$^3J_{H5,NH}$	9.2	obsc	9.4	nm
$^3J_{H5,H6}$	obsc	obsc	10.3	10.5
$^3J_{H6,H7}$	obsc	obsc	1.2	1.2
$^3J_{H7,H8}$	obsc	obsc	9.3	9.1
$^3J_{H8,H9}$	obsc	obsc	2.8	2.7
$^3J_{H8,H9'}$	obsc	obsc	6.4	6.4
$^2J_{H9,H9'}$	obsc	obsc	−11.9	−11.9

[a] In Hz ± 0.1 Hz at ~25 °C; obsc denotes obscured signal; nm denotes not measureable.

TABLE 2. Calculated $^1H-^1H$ Spin-Coupling Constants in 7–10[a]

	compd			
J-coupling (Hz)	$\mathbf{7}^{FXS}$	$\mathbf{8}^{FXS}$	$\mathbf{9}^{FXS}$	$\mathbf{10}^{FXS}$
$^3J_{H3ax,H4}$	12.0 (11.4)	11.7 (11.4)	11.5 (11.4)	11.8 (11.5)
$^3J_{H3eq,H4}$	5.2 (4.6)	5.2 (~4.1)	5.3 (4.9)	5.4 (4.9)
$^2J_{H3ax,H3eq}$	−13.0 (−12.8)	−11.8 (−12.5)	−12.9 (−13.1)	−13.1 (−13.0)
$^3J_{H4,H5}$	10.0	9.8	9.9 (10.1)	9.8 (9.9)
$^3J_{H5,NH}$	(9.2)		(9.4)	
$^3J_{H5,H6}$	10.6	10.5	10.7 (10.3)	10.7 (10.5)
$^3J_{H6,H7S}$	1.8	1.9	1.9 (1.2)	1.9 (1.2)

[a] Reported couplings were obtained by averaging the couplings calculated in the 12 C1−C2 rotamers of each structure. Experimental values are shown in parentheses.

TABLE 3. $^{13}C-^1H$ Spin-Coupling Constants in 2 at p^2H 2.0 and pH 8.0[a]

	2α*p*		2β*p*	
J-coupling (Hz)	p^2H 2.0	pH 8.0	p^2H 2.0	pH 8.0
$^3J_{C1,H3ax}$	7.0	6.2	1.6	1.0
$^3J_{C1,H3eq}$	~0	~0	~0	~0
$^2J_{C2,H3ax}$	±7.7	±7.4	±3.6	±3.4
$^2J_{C2,H3eq}$	~± 4.3	~± 4.1	±3.9	±3.5
$^3J_{C2,H4}$	obsc	obsc	0.5	nc
$^3J_{C2,H6}$	obsc	obsc	~1.3	1.2
$^4J_{C2,H7}$	obsc	obsc	0.8	br
$^1J_{C3,H3ax}$	129.4	~128.3	129.8	129.1
$^1J_{C3,H3eq}$	134.1	~133.5	133.5	132.5
$^2J_{C3,H4}$	obsc	obsc	~± 2.1	±2.1
$^3J_{C3,H5}$	obsc	obsc	1.0	nm

[a] In Hz ± 0.1 Hz; obsc denotes obscured signal; nm denotes not measureable; br denotes broadened signal; nc denotes no coupling (J < 0.6 Hz).

J-Couplings were calculated in *Gaussian*03 using DFT (B3LYP) and a [5s2p1d,3s1p] basis set.[14b] The reported couplings contain both Fermi and non-Fermi contact contributions and are unscaled. The effect of solvent–water on the computed couplings (series 3 and 4) was evaluated using the Self-Consistent Reaction Field (SCRF)[14c] and the Integral Equation Formalism (polarizable continuum) model (IEFPCM)[14d] and the [5s2p1d,3s1p] basis set as implemented in *Gaussian*03. Average *J*-couplings reported in Tables 2, 4, 6, and 8 are unweighted, since energies calculated for the 12 C1−C2 rotamers were not considered sufficiently quantitative to warrant a weighted treatment. This simplification introduces uncertainties when comparing calculated and experimental couplings.

(10) Frisch, M. J., et al. *Gaussian*03, Revision A.1; Gaussian, Inc.: Pittsburgh, PA, 2003.
(11) Becke, A. D. *J. Chem. Phys.* **1993**, *98*, 5648–5652.
(12) Hehre, W. J.; Ditchfield, R.; Pople, J. A. *J. Chem. Phys.* **1972**, *56*, 2257–2261.
(13) Pan, Q.; Klepach, T.; Carmichael, I.; Reed, M.; Serianni, A. S. *J. Org. Chem.* **2005**, *70*, 7542–7549.
(14) (a) Zhao, H.; Pan, Q.; Zhang, W.; Carmichael, I.; Serianni, A. S. *J. Org. Chem.* **2007**, *72*, 7071–7082. (b) Stenutz, R.; Carmichael, I.; Widmalm, G.; Serianni, A. S. *J. Org. Chem.* **2002**, *67*, 949–958. (c) Cancés, M. T.; Mennucci, B.; Tomasi, J. *J. Chem. Phys.* **1997**, *107*, 3032. (d) Cammi, R.; Mennucci, B.; Tomasi, J. *J. Phys. Chem. A* **2000**, *104*, 5631.

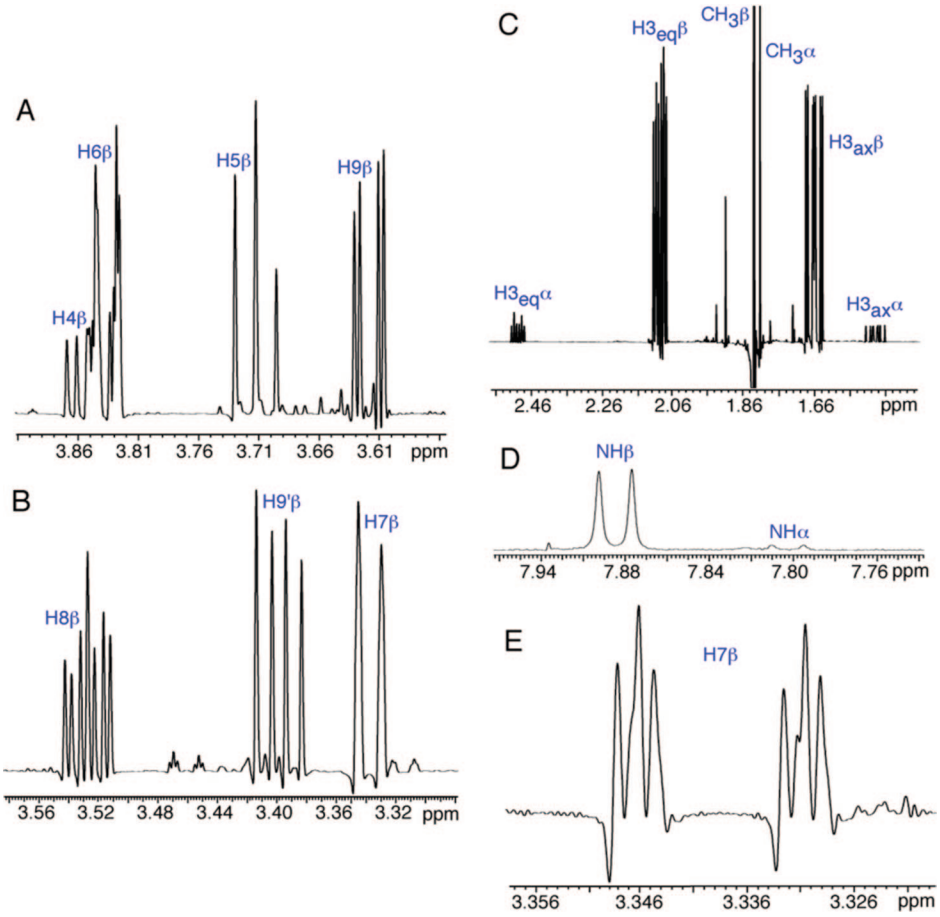

FIGURE 1. Expanded regions of the resolution-enhanced ^{1}H NMR spectrum of [2-^{13}C]**2** at p^{2}H 2.0 and 25 °C showing signal assignments. The amide signals in (D) were very weak due to the small percentage of molecules containing ^{1}H at the NH site in ^2H_2O. The H7β signal in (B) is expanded in (E) to show the presence of two $^3J_{HH}$ and the long-range $^4J_{C2,H7}$.

TABLE 4. Calculated ^{13}C−^{1}H Spin-Coupling Constants in 7–10[a]

	compd			
J-coupling (Hz)	**7**^{FXS}	**8**^{FXS}	**9**^{FXS}	**10**^{FXS}
$^3J_{C1,H3ax}$	7.4 (7.0)	5.5 (6.2)	2.0 (1.6)	1.6 (1.0)
$^3J_{C1,H3eq}$	1.5 (∼0)	1.0 (∼0)	0.5 (∼0)	0.5 (∼0)
$^2J_{C2,H3ax}$	−7.0 (−7.7)	−6.2 (−7.4)	−2.7 (−3.6)	−3.0 (−3.4)
$^2J_{C2,H3eq}$	−2.3 (∼−4.3)	−2.1 (∼−4.1)	−2.7 (−3.9)	−2.5 (−3.5)
$^3J_{C2,H4}$	0.7	0.7	0.7 (0.5)	0.6 (nc)
$^3J_{C2,H6}$	1.0	1.2	1.8 (∼1.3)	1.8 (1.2)
$^4J_{C2,H7}$	1.5	1.2	1.0 (0.8)	0.7 (br)
$^1J_{C3,H3ax}$	133.1 (129.4)	130.4 (∼128.3)	132.0 (129.8)	130.4 (129.1)
$^1J_{C3,H3eq}$	138.3 (134.1)	135.4 (∼133.5)	138.4 (133.5)	135.2 (132.5)
$^2J_{C3,H4}$	−1.5	−1.8	−1.7 (∼−2.1)	−1.7 (−2.1)
$^3J_{C3,H5}$	1.9	1.8	1.7 (1.0)	1.6 (nm)

[a] Reported couplings were obtained by averaging the couplings calculated in the 12 C1−C2 rotamers of each structure. Experimental values are shown in parentheses; nc denotes no coupling (J < 0.6 Hz); br denotes broadened signal; nm denotes not measureable.

Results and Discussion

A. General Considerations. The ^{1}H NMR spectrum of Neu5Ac is dominated by signals arising from **2**βp (Figure 1);[15–17] signal assignments are given in Table S1 at p^{2}H 2.0 and pH 8.0. The detection of **2**αp was difficult, and only $H3_{ax}$, $H3_{eq}$, and the *N*-acetyl methyl protons could be assigned with confidence to this form. In **2**αp and **2**βp, the $H3_{ax}$ signal is more shielded than that of $H3_{eq}$, and the difference in their chemical shifts is more pronounced for **2**αp (∼1 ppm) than for **2**βp (∼0.4 ppm). ^{1}H signals arising from the exchangeable NH protons of the *N*-acetyl side chain were observed at ∼8 ppm, appearing as a weak doublet at p^{2}H 2.0 and an exchange-broadened singlet at pH 8.0 (Figure S1). The effect of amide proton exchange was also evident at the H5β signal, which appeared as a slightly broadened triplet at p^{2}H 2.0, and an exchange-broadened triplet at pH 8.0 in unlabeled **2** (Figure S2).

^{1}H NMR spectra of **2**$^{1-3}$ were initially obtained at p^{2}H 2.0 and p^{2}H 8.0. While the former spectra were interpretable (Figure 1) and are discussed below, the latter spectra were devoid of $H3_{ax}/H3_{eq}$ signals and contained a doublet for the H4 signal of **2**βp, when solutions were allowed to stand for an extended time prior to analysis. Similar effects were observed in ^{13}C NMR spectra at p^{2}H 8.0, with the C3 signals being difficult to detect under these conditions. Further investigation confirmed that solvent deuterium exchange at C3 is facile in alkaline solutions (Scheme S3), with more rapid exchange observed for $H3_{ax}$ than for $H3_{eq}$ in **2**αp and **2**βp.[16] The *J*-coupling studies at high pH reported herein were conducted in 95/5 (v/v) $H_2O/^2H_2O$ solvent to eliminate this complication.

The ^{13}C NMR spectrum of **2** (Figure 2) contained well-resolved signals for both pyranoses,[17–20] allowing complete signal assignments at p^{2}H 2.0 and pH 8.0 (Table S2). ^{13}C{^{1}H}

(15) Brown, E. B.; Brey, W. S.; Weltner, W. *Biochim. Biophys. Acta* **1975**, *399*, 124–130.
(16) Schmidt, H.; Friebolin, H. *J. Carbohydr. Chem.* **1983**, *2*, 405–413.
(17) Gervay, J.; Batta, G. *Tetrahedron Lett.* **1994**, *35*, 3009–3012.
(18) Czarniecki, M.; Thornton, E. R. *J. Am. Chem. Soc.* **1976**, *98*, 1023–1025.

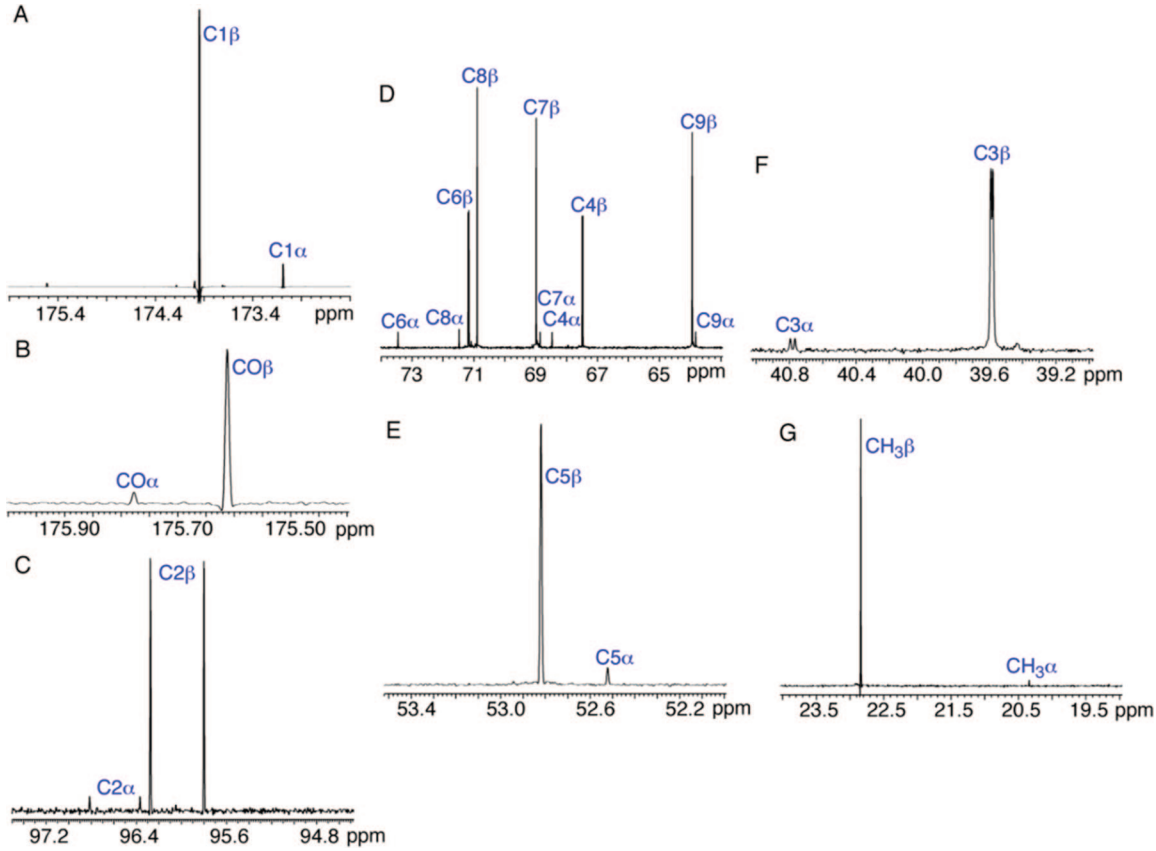

FIGURE 2. Expanded regions of the $^{13}C\{^1H\}$ NMR spectrum of [1-^{13}C]**2** at p^{2}H 2.0 and 25 °C. The C2 signals (C) show the presence of the large $^1J_{C1,C2}$, and smaller, longer-range couplings are observed at C6β ($^3J_{C1,C6}$) (D) and C3α/β ($^2J_{C1,C3}$) (F).

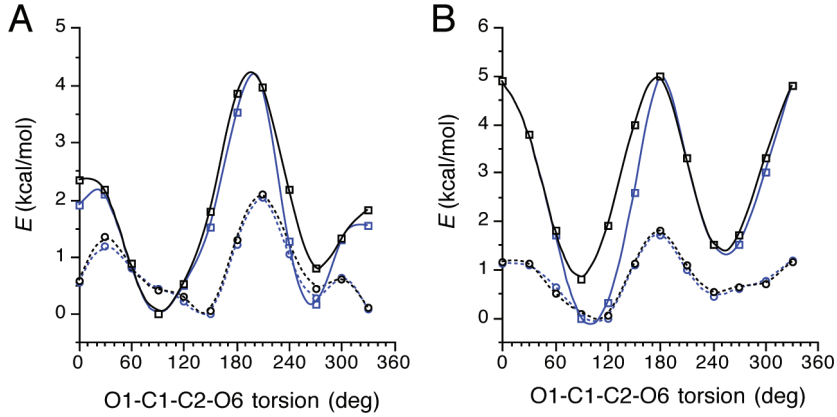

FIGURE 3. Effect of C1−C2 bond rotation on the total energies of protonated **7** (A) and **9** (B). *In vacuo* data are shown as solid lines, and solvated (water) data are shown as dotted lines. Black symbols = FX series; blue symbols = FL series.

NMR spectra of **2**^{1}, **2**^{2}, and **2**^{3} contained doublets due to $^1J_{CC}$ which were used to confirm the C1−C4 signal assignments. The C5−C7 signals were assigned based on an analysis of longer-range J_{CC}. The C8 and C9 signals were assigned based on the expected chemical shift differences for 1° and 2° alcoholic carbons in saccharides; these assignments for **2**βp were consistent with those made by Gervay and Batta ($\delta_{C6} > d_{C8} > \delta_{C7} > \delta_{C4} > \delta_{C9}$).[17]

B. Conformational Properties of the C1−C2 Bond. The energetics of C1−C2 bond rotation in **2** was investigated by DFT since this rotation could affect *J*-couplings involving carbons and protons near the carboxyl group.

The effect of C1−C2 bond rotation in protonated **2**αp and **2**βp on total energy is shown in Figure 3. *In vacuo* energy profiles show significantly larger amplitudes than solvated profiles. The effect of fixing the C2−O2 bond torsion is small, with observed differences possibly caused by H-bonding in some of the *in vacuo* conformations. This H-bonding is presumably suppressed in the corresponding solvated conformations. For **2**βp, *in vacuo* and solvated data show the same global minimum at ~90° and a local minimum at ~−90°. The dampened barriers

(19) (a) Czarniecki, M.; Thornton, E. R. *J. Am. Chem. Soc.* **1977**, *99*, 8273–8279. (b) Hori, H.; Nakajima, T.; Nishida, Y.; Ohrui, H.; Meguro, H. *Tetrahedron Lett.* **1988**, *29*, 6317–6320.

(20) (a) Szarek, W. A.; Roszak, A. W.; Crone, G. M.; Martin, O. R. *Acta Crystallogr.* **1997**, *C53*, 1921–1923. (b) O'Connell, A. M. *Acta Crystallogr.* **1973**, *B29*, 2320–2328.

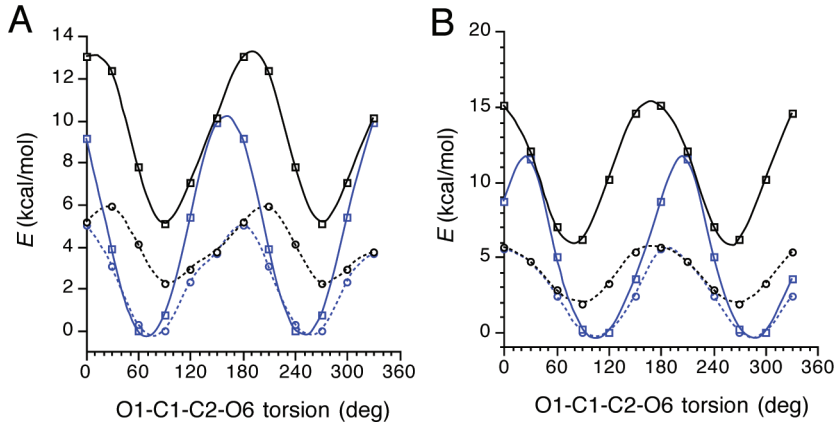

FIGURE 4. Effect of C1−C2 bond rotation on total energies of **8** (A) and **10** (B). *In vacuo* data are shown as solid lines, and solvated (water) data are shown as dotted lines. Black symbols = FX series; blue symbols = FL series.

in the solvated data suggest considerable conformational sampling. For **2**α*p*, *in vacuo* and solvated data differ with respect to the location of the global minimum and the shape of the curve near this minimum. The solvated data suggest that torsions between 90° and 150° and between 0° and −90°, are nearly isoenergetic, with the global minimum at ∼150°. Conformational heterogeneity about the C1−C2 bond appears greater in **2**α*p* than in **2**β*p*. In **2**α*p*, multiple steric interactions between the COOH group and the pyranose ring are possible and exert a leveling effect on the energetics, whereas in **2**β*p*, the equatorial COOH group is subject to less steric interactions and is thus more likely to favor a more limited set of conformations.

Energy curves for the carboxylate anions are shown in Figure 4. As observed in the COOH forms, inclusion of solvent dampens curve amplitude substantially, but barrier heights appear generally greater for COO^- forms than for COOH forms. Phase-shifting (defined as systematic shifting of minima and maxima along the *x*-axis of the plot) for **2**β*p* is more apparent between the FX and FL series and is still observable in the FXS and FLS data sets. Phase-shifting is observed in ionized **2**α*p* in both the *in vacuo* and solvated data, whereas it is absent in the protonated form. For **2**β*p*, well-defined minima were observed at approximately 90°−120° and 260°−300°. For **2**α*p*, minima were located at approximately 60°−90° and 240°−270°.

Preferred C1−C2 conformations in **2**α*p* and **2**β*p* are summarized in Scheme S4, with the caveat that, in both structures, significant averaging about the C1−C2 bond probably occurs in solution, particularly for the protonated forms.

C. ^{1}H−^{1}H Spin-Couplings. ^{1}H−^{1}H Spin-couplings in **2**β*p* range from 1.2 to 11.5 Hz for $^3J_{HH}$ and –11.9 to –13.1 Hz for $^2J_{HH}$ (Table 1). The large intraring $^3J_{H3ax,H4}$, $^3J_{H4,H5}$, and $^3J_{H5,H6}$ correspond to *anti* arrangements of the coupled hydrogens, consistent with a preferred $^2C_5$ ring conformation. The small $^3J_{H6,H7}$ (1.2 Hz) and large $^3J_{H7,H8}$ (9.1–9.3 Hz) are noteworthy, with the former suggesting a preferred *gauche*/orthogonal torsion angle between H6 and H7 and the latter suggesting a preferred near-*anti* arrangement between H7 and H8. These couplings place significant constraints on exocyclic glycerol side-chain conformation,[15] which will be discussed below when J_{CH} and J_{CC} are considered. The magnitudes of the J_{HH} values in **2**β*p* are largely independent of ionization state even for couplings involving nuclei close to the site of ionization (e.g., $H3_{ax/eq}$). The available J_{HH} values in **2**α*p* are similar in magnitude to those observed in **2**β*p*.

Doublets were observed at ∼7.8 ppm for the NH protons of **2**α*p* and **2**β*p* at p^{2}H 2.0 (Figure 1D). $^3J_{H5,NH}$ values of 9.2 and 9.4 Hz were measured for **2**α*p* and **2**β*p*, respectively. These couplings are assumed to be minimally affected by exchange broadening since NH exchange with solvent–water was slow under the conditions used for these determinations.

Computed ^{1}H−^{1}H couplings (Table 2) show good agreement with the experimental couplings. For example, computed couplings in **9** are within 0.1–0.4 Hz of experimental values except for $^3J_{H6,H7S}$. The slightly larger deviation for $^3J_{H6,H7S}$ is likely caused by differences in exocyclic side chain covalent structure and/or in the C6−C7 bond torsions in **2**β*p* and **9** (note that H7*S* of **9**/**10** corresponds to H7 of **2**β*p*).

D. ^{13}C−^{1}H Spin-Couplings. Vicinal ^{13}C−^{1}H couplings between C1 and $H3_{ax}/H3_{eq}$ differ in **2**α*p* and **2**β*p* as described previously.[19a,b] In **2**α*p*, $^3J_{C1,H3ax}$ is large (6.2/7.0 Hz) (Table 3), indicative of an *anti* arrangement, whereas $^3J_{C1,H3eq}$ is essentially zero, consistent with a *gauche* arrangement. In **2**β*p*, both *gauche* couplings are <1.6 Hz. The three *gauche* couplings are nonequivalent, with $^3J_{C1,H3ax}$ in **2**β*p* larger than $^3J_{C1,H3eq}$ in **2**α*p* and **2**β*p* at p^{2}H 2.0 and pH 8.0. Newman projections about the C2−C3 bond (Scheme 3) show the presence of an electronegative substituent *anti* to all three of the *gauche*-coupled C3 protons, so an *anti* effect cannot explain the observed results. The ring oxygen O6 may be more effective at reducing *gauche* $^3J_{CCCH}$ than O2 due to different stereoelectronic properties at the two oxygens. Potential substituent effects caused by the presence of the C1 carboxyl group were investigated through studies of 3-deoxy-β-D-[1-^{13}C]fructopyranose **11**, a structural analogue of **2**β*p*. In **11**, $^3J_{C1,H3ax/eq}$ values are similar to those in **2**β*p*. Alternatively, the different *gauche* couplings may be caused by slightly different C−C−C−H torsion angles in the chair forms of **2**α*p*, **2**β*p*, and **11**. Inspection of crystal structures of **11**[20a] and the methyl ester of **2**β*p*[20b] gives C1−C2−C3−$H3_{ax}$ torsions of –49.2°/−46.7° and C1−C2−C3−$H3_{eq}$ torsions of 68.6°/61.9°. If similar torsions are present in solution, they would produce *gauche* $^3J_{C1,H3ax}$ values larger than *gauche* $^3J_{C1,H3eq}$values, consistent with the experimental observations.

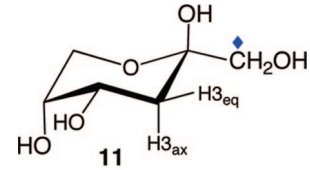

11

$^3J_{C1,H3ax}$ = 1.8 Hz
$^3J_{C1,H3eq}$ = 0.4 Hz

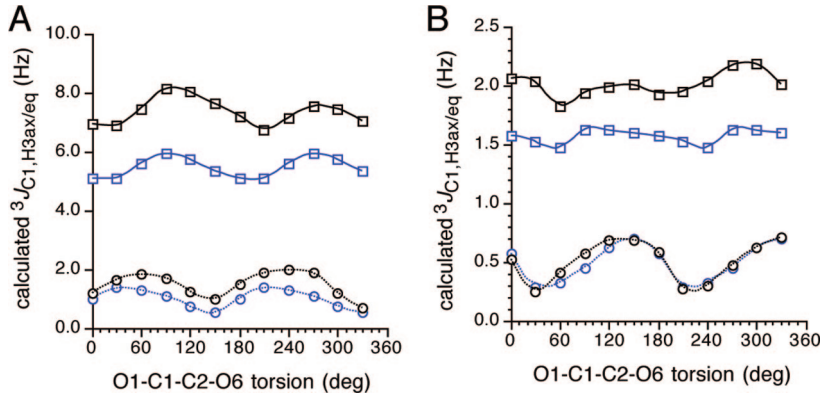

FIGURE 5. Effect of C1−C2 bond rotation on calculated $^3J_{C1,H3ax/eq}$ in **7/8** (A) and **9/10** (B). Squares = $H3_{ax}$, circles = $H3_{eq}$. Black symbols = protonated form; blue symbols = ionized form. Data taken from the FXS series.

SCHEME 3. Projections for $^3J_{C1,H3ax}$ and $^3J_{C1,H3eq}$ in 2α*p* and 2α*p*

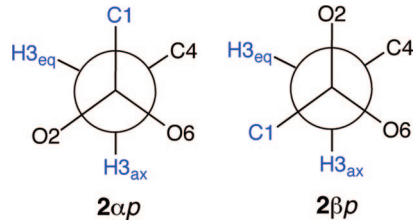

TABLE 5. $^{13}C-^{13}C$ Spin-Coupling Constants[a] in 2 at p^{2}H 2.0 and pH 8.0

	2α*p*		2β*p*	
J-coupling (Hz)	p^{2}H 2.0	pH 8.0	p^{2}H 2.0	pH 8.0
$^1J_{C1,C2}$	67.4	62.6	71.7	66.3
$^2J_{C1,C3}$	±4.1	±3.8	∼± 1.7	±1.4
$^3J_{C1,C4}$	0	0	3.3	3.1
$^3J_{C1,C6}$	0	0	3.3	3.1
$^1J_{C2,C3}$	41.7	42.3	41.0	41.1
$^2J_{C2,C4}$	0 or br		±1.5	±1.5
$^2J_{C2,C6}$	br	0	±1.9	±2.1
$^{3+3}J_{C2,C5}$	0	0	0	0
$^3J_{C2,C7}$	3.5	3.6	3.2	3.1
$^1J_{C3,C4}$	35.8		35.8	35.6
$^2J_{C3,C5}$	0	0	0	0
$^{3+3}J_{C3,C6}$	0 or br	0	0	0

[a] ln Hz ± 0.1 Hz; obsc denotes obscured signal; br denotes broadened signal.

Calculated $^3J_{C1,H3ax/eq}$ in **7** and **9** (Table 4) are in moderate agreement with the experimental findings. In **7**, $^3J_{C1,H3ax}$ and $^3J_{C1,H3eq}$ are 7.4 and 1.5 Hz, respectively, whereas in **9**, the respective couplings are 2.0 and 0.5 Hz. These data display the expected relative couplings in **9**, but $^3J_{C1,H3eq}$ is larger than expected in **7**. However, the magnitudes of these $^3J_{CCCH}$ depend on C1−C2 bond conformation (Figure 5), making quantitative comparisons between computed and experimental couplings difficult. Ionization of the COOH group generally reduces experimental $^3J_{C1,H3ax/eq}$ (Table 3), and a similar shift to smaller couplings is observed in the calculated couplings (Table 4).

Like $^3J_{C1,H3ax/eq}$, $^2J_{C2,H3ax}$ and $^2J_{C2,H3eq}$ can be used to distinguish between **2**α*p* and **2**β*p* (Table 3). $^2J_{C2,H3ax} > {}^2J_{C2,H3eq}$ in **2**α*p*, whereas $^2J_{C2,H3ax} \approx {}^2J_{C2,H3eq}$in **2**β*p*. Application of the projection rule[21](Scheme S5) yields projections of +0.5 for both couplings in **2**β*p* and for $^2J_{C2,H3eq}$ in **2**α*p*, whereas the projection for $^2J_{C2,H3ax}$ in **2**α*p* is –1.0. Projections of +0.5 and –1.0 correlate with ∼0 and very negative values of $^2J_{CCH}$, respectively. The large $^2J_{C2,H3ax}$ in **2**α*p* is thus probably negative, but the projection rule cannot predict the remaining signs reliably. Since C2 is unprotonated, $^1H-^1H$ TOCSY data could not be used to determine the signs.[22] Therefore, DFT calculations were used to make these determinations.

TABLE 6. Calculated $^{13}C-^{13}C$ Spin-Coupling Constants[a] in 7−10

	compd			
J-coupling (Hz)	**7**^{FXS}	**8**^{FXS}	**9**^{FXS}	**10**^{FXS}
$^1J_{C1,C2}$	73.1 (67.4)	66.4 (62.6)	80.0 (71.7)	70.4 (66.3)
$^2J_{C1,C3}$	+4.9 (+4.1)	+4.1 (+3.8)	+2.1 (+1.7)	+1.9 (+1.4)
$^3J_{C1,C4}$	−0.2 (0)	−0.2 (0)	3.4 (3.3)	2.7 (3.1)
$^3J_{C1,C6}$	−0.2 (0)	−0.1 (0)	4.1 (3.3)	3.1 (3.1)
$^1J_{C2,C3}$	43.7 (41.7)	43.8 (42.3)	44.9 (41.0)	45.8 (41.1)
$^2J_{C2,C4}$	+1.5 (*br*)	+1.7	−1.1 (−1.5)	−1.4 (−1.5)
$^2J_{C2,C6}$	−1.7 (*br*)	−1.3 (0)	−1.9 (−1.9)	−2.6 (−2.1)
$^{3+3}J_{C2,C5}$	0.3 (0)	0.3 (0)	0.3 (0)	0.3 (0)
$^3J_{C2,C7}$	4.0 (3.5)	3.7 (3.6)	3.9 (3.2)	3.5 (3.1)
$^1J_{C3,C4}$	36.3 (35.8)	36.7	36.0 (35.8)	36.4 (35.6)
$^2J_{C3,C5}$	2.1 (0)	1.9 (0)	2.1 (0)	2.0 (0)
$^{3+3}J_{C3,C6}$	0.1 (br)	0.1 (0)	0.3 (0)	0.4 (0)

[a] Reported couplings were obtained by averaging the couplings calculated in the 12 C1−C2 rotamers of each structure. Experimental values are shown in parentheses; br denotes broadened signals.

Negative signs were obtained for $^2J_{CH}$ involving C2 and $H3_{ax/eq}$ in **7−10** (Table 4). Experimental coupling trends were maintained in the calculations, with very different couplings observed in **7/8** compared to **9/10**. These geminal couplings show differential sensitivities to rotation of the C1−C2 bond, with the large $^2J_{C2,H3ax}$ in **7** much less sensitive than the remaining three couplings (Figure 6). $^2J_{C2,H3}$ values involving the C3 protons closest to the COOH group ($H3_{eq}$ in **7/8**; $H3_{ax/eq}$ in **9/10**) appear more affected by its rotation than $^2J_{C2,H3}$ values involving protons farther away ($H3_{ax}$ in **7/8**). The underlying mechanisms responsible for this behavior are unclear.

$^3J_{C2,H4}$ is small in **2**β*p* (0.5 Hz) and corresponds to a C2−C3−C4−H4 torsion angle of ∼−60°; the computed coupling is 0.7 Hz. This coupling is consistent with the analogous $^3J_{C1,H3}$ in D-aldopyranosyl rings ($^4C_1$), which varies from 0 to 1.3 Hz.[22] $^3J_{C2,H6}$ in **2**β*p* (∼1.2 Hz) is also consistent with a C2−O6−C6−H6 torsion angle of ∼+60° and is comparable to $^3J_{C1,H5}$ in D-aldopyranosyl rings ($^4C_1$) (∼2.0 Hz).[22] Computed $^3J_{C2,H6}$ values of 1.2 and 1.8 Hz were obtained in **8** and **10**, respectively, in reasonable agreement with

(21) Bock, K.; Pedersen, C. *Acta Chem. Scand.* **1977**, *B31*, 354–358.
(22) Podlasek, C. A.; Wu, J.; Stripe, W. A.; Bondo, P. B.; Serianni, A. S. *J. Am. Chem. Soc.* **1995**, *117*, 8635–8644.

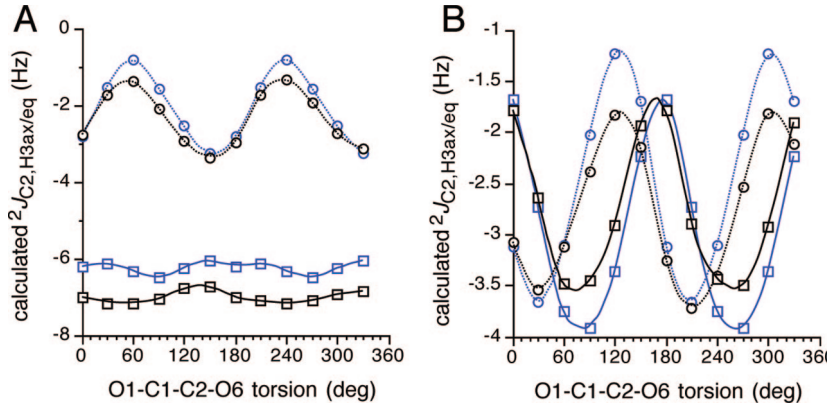

FIGURE 6. Effect of C1−C2 bond rotation on calculated $^2J_{C2,H3eq/ax}$ in **7/8** (A) and **9/10** (B). Squares = $H3_{ax}$, circles = $H3_{eq}$. Black symbols = protonated form; blue symbols = ionized form. Data taken from the FXS series.

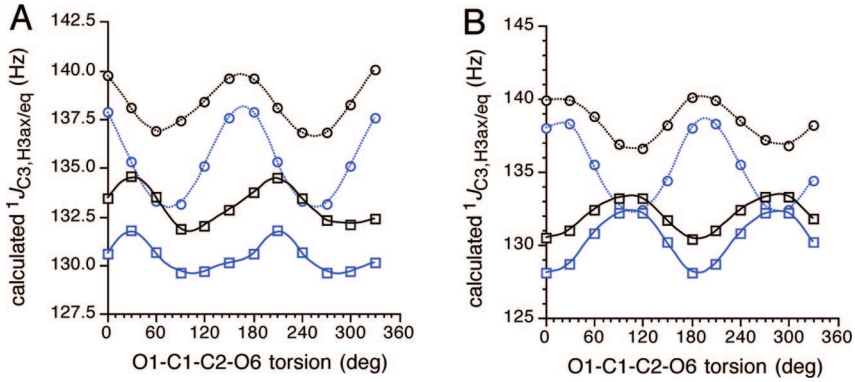

FIGURE 7. Effect of C1−C2 bond rotation on calculated $^1J_{C3,H3eq/ax}$ in **7/8** (A) and **9/10** (B). Squares = $H3_{ax}$, circles = $H3_{eq}$. Black symbols = protonated form; blue symbols = ionized form. Data taken from the FXS series.

experiment. C2 is also coupled to H7 in **2**βp (Figure 1E). This long-range $^4J_{COCCH}$ is related to $^4J_{C1,H6R/S}$ values involving the exocyclic hydroxymethyl protons of some aldohexopyranosyl rings,[23] and its presence constrains conformation about the C6−C7 bond (see discussion below).

$^1J_{C3,H3eq}$ is ∼4 Hz larger than $^1J_{C3,H3ax}$ in **2**αp and **2**βp. The equatorial C3−H3 bond is expected to be shorter than the axial C3−H3 bond, and the resulting enhanced *s*-character is expected to produce a larger $^1J_{CH}$.[24] Both $^1J_{CH}$ are relatively insensitive to the COOH ionization state (changes of 1.1 Hz or less).

DFT calculations show $^1J_{C3,H3ax/eq}$ to be sensitive to C1−C2 bond conformation in **2**αp and **2**βp (Figure 7). The sensitivity is largest for $^1J_{C3,H3eq}$ in the ionized form of both anomers, showing a change of 5–7 Hz as the bond is rotated. DFT calculations also predict a decrease in both couplings upon COOH ionization and, in general, larger couplings for the C3−$H3_{eq}$ bonds. The *relative* difference between $^1J_{C3,H3ax}$ and $^1J_{C3,H3eq}$, however, is predicted to depend on C1−C2 bond conformation, with some conformations of **2**βp giving identical couplings in the COO^- form.

$^2J_{C3,H4}$ is ∼2.1 Hz in **2**βp, and the projection rule[21] yields a projection of +0.5. This coupling is expected to be negative since the analogous $^2J_{C2,H3}$ in the 2-deoxy-α-D-glucopyranosyl ring is –2.0 Hz (projection of +0.5).[25] This expectation is confirmed by the DFT calculations (Table 4). The *gauche* $^3J_{C3,H5}$ in **2**βp of 1.0 Hz is similar to the *gauche* $^3J_{C2,H4}$ observed in 2-deoxy-α-D-glucopyranosyl (∼0 Hz) and 2-deoxy-β-D-allopyranosyl (∼0 Hz) rings.[25]

E. ^{13}C−^{13}C Spin-Couplings. $^1J_{C1,C2}$ in **2**αp and **2**βp range from 62.6 to 71.7 Hz and depend on anomeric configuration, with **2**αp giving smaller couplings by ∼4 Hz (Table 5). Solution pH influences $^1J_{C1,C2}$, with couplings ∼5 Hz smaller in the ionized forms. If the *s*-character of the C1−C2 bond largely determines $^1J_{C1,C2}$, then the smaller coupling in the ionized state implies less *s*-character. The latter should lead to a longer C1−C2 bond. DFT calculations confirm this expectation (Figure 8), with $r_{C1,C2}$ being consistently shorter in the protonated forms by ∼0.03 and ∼0.02 Å in *in vacuo* and solvated calculations, respectively. C1−C2 bond length also varies somewhat with C1−C2 bond rotation, with **2**αp showing a more systematic dependence in both its protonated and ionized forms.

DFT calculations show that $^1J_{C1,C2}$ scales inversely with $r_{C1,C2}$, with larger couplings observed in the protonated forms (Figure 9). $^1J_{C1,C2}$ is smaller in the ionized forms, and the amount of decrease depends on whether the calculations were conducted *in vacuo* or with solvent. The solvated data are in closer agreement with experiment, suggesting that neglecting solvent accentuates (localizes) the charged properties of the carboxylate anion, which in turn produces hyper-extension of $r_{C1,C2}$ and hyper-reduction of $^1J_{C1,C2}$. A hyperconjugative mechanism may explain $r_{C1,C2}$ elongation in the anion (Scheme 4), where contributions from resonance structure **II** are responsible for weakening (lengthening) the C1−C2 bond in the anion and for concomitant reduction in $^1J_{C1,C2}$.

(23) Pan, Q.; Klepach, T.; Carmichael, I.; Reed, M.; Serianni, A. S. *J. Org. Chem.* **2005**, *70*, 7542–7549.
(24) Klepach, T.; Carmichael, I.; Serianni, A. S. *J. Am. Chem. Soc.* **2005**, *127*, 9781–9793.
(25) Bose, B.; Serianni, A. S., unpublished results.

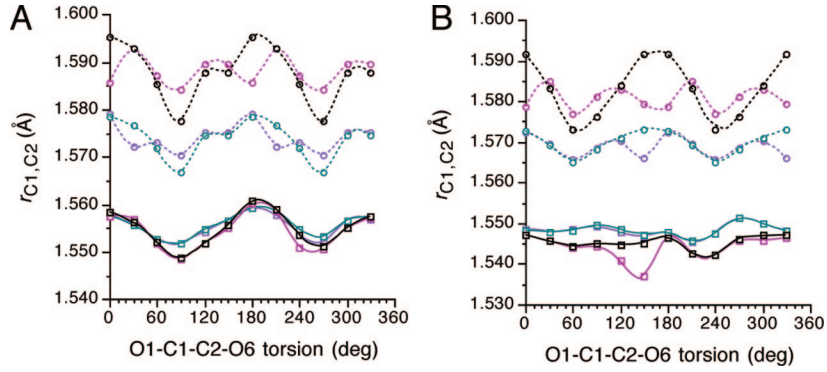

FIGURE 8. Effect of C1−C2 bond rotation on $r_{C1,C2}$ in **7/8** (A) and **9/10** (B). Squares = protonated form; circles = ionized form. Black/red symbols = FX/FL series; green/purple symbols = FXS/FLS series.

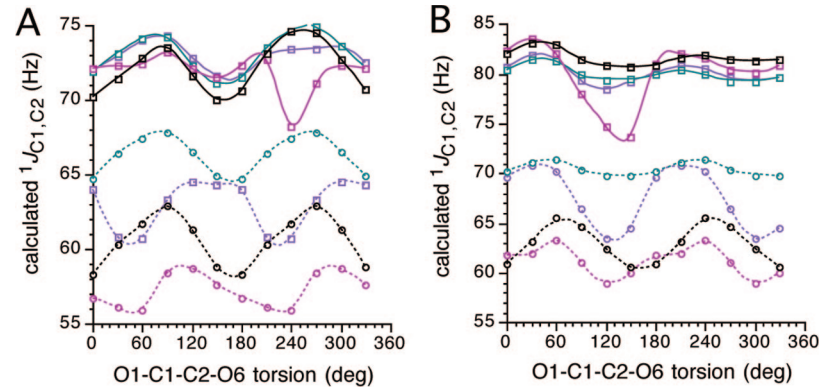

FIGURE 9. Effect of C1−C2 bond rotation on $^1J_{C1,C2}$ in **7/8** (A) and **9/10** (B). Squares = protonated form; circles = ionized form. Black/red symbols = FX/FL series; green/purple symbols = FXS/FLS series.

TABLE 7. J_{CC} **Values**[a] **in 2**βp**, 3-Deoxy-**β**-D-fructopyranose 11, and** β**-D-Fructopyranose 12**

J-coupling (Hz)	**11**	**12**[b]	**2**$\beta\rho$[c]
$^1J_{C1,C2}$	50.2	49.8	71.7
$^2J_{C1,C3}$	±3.4	±2.4	∼+1.7
$^3J_{C1,C4}$	2.7	1.8	3.3
$^3J_{C1,C6}$	2.7	2.4	3.3
$^1J_{C2,C3}$		47.5	41.0
$^2J_{C2,C4}$		nc	−1.5
$^2J_{C2,C6}$		±2.1	−1.9
$^1J_{C3,C4}$		39.8	35.8
$^2J_{C3,C5}$		nc	0

[a] In Hz ± 0.1 Hz; nc denotes no coupling (J < 0.6 Hz). [b] Data taken from ref 29. [c] At pH 2.0; data from Table 5.

$^2J_{C1,C3}$ depends on anomeric configuration, with absolute couplings in **2**αp larger than in **2**βp by ∼2 Hz. The projection resultant method[26] could not be used to predict their signs due to the sp^2 character of C1, but DFT calculations predict positive signs for $^2J_{C1,C3}$ in **2**αp and **2**βp (Table 6), a dependence on anomeric configuration that mirrors the experimental findings, and a dependence on the C1−C2 torsion angle, especially in the protonated state (Figure 10A). $^2J_{C1,C3}$ may be slightly reduced in the ionized state (Table 5), which is also suggested from the calculations.

$^3J_{C1,C4}$and $^3J_{C1,C6}$ differ significantly in **2**αp and **2**βp, with essentially zero couplings observed in the former and 3.1–3.3 Hz couplings observed in the latter (Table 5). These couplings show a small dependence on COOH ionization state. Similar trends are predicted by DFT (Table 6), and both vicinal couplings show little dependence on C1−C2 bond rotation (data not shown). The 3.1–3.3 couplings in **2**βp correspond to C1−C2−C3−C4 and C1−C2−O6−C6 torsion angles of ∼180°, and the ∼0 Hz couplings in **2**αp correspond to torsion angles of ∼± 60°. Anti couplings $^3J_{C1,C4}$ and $^3J_{C1,C6}$ in **2**βp are virtually identical, implying that oxygen along the coupling pathway exerts a minimal effect on the coupling (crystallographic data for the methyl ester of **2**βp[20b] shows C1−C2−C3−C4 and C1−C2−O6−C6 torsion angles of –170.3° and –177.5°, respectively). This behavior is similar to that of $^3J_{C1,C6}$ and $^3J_{C3,C6}$ in aldohexopyranosyl rings, which exhibit a similar Karplus dependency.[27]

$^1J_{C2,C3}$ ranges from 41.0 to 42.3 Hz and shows little sensitivity to anomeric configuration and to COOH ionization state. $^1J_{C2,C3}$ depends on the C1−C2 bond torsion (Figure 10B), with maximal couplings observed at ∼120° and ∼300° in **2**αp and ∼60° and ∼240° in **2**βp for both the protonated and ionized states.

$^2J_{C2,C4}$ is very small in **2**αp, slightly larger in **2**βp, and is not significantly affected by ionization at C1. DFT computations predict a positive sign in **2**αp and a negative sign in **2**βp (Table 6). The sensitivity of $^2J_{C2,C4}$ to C1−C2 bond rotation (Figure 11A) is significantly greater in **2**αp than in **2**βp and may explain the apparent greater disparity between computed and experimental $^2J_{C2,C4}$ in **2**αp (Table 6).

Like $^2J_{C2,C4}$, $^2J_{C2,C6}$is larger in **2**βp than in **2**αp, and DFT calculations indicate negative signs in both anomers (Table 6).

(26) Church, T.; Carmichael, I.; Serianni, A. S. *Carbohydr. Res.* **1996**, *280*, 177–186.

(27) Bose, B.; Klepach, T.; Bondo, G.; Bondo, P. B.; Zhang, W.; Carmichael, I.; Serianni, A. S. *J. Org. Chem.* **2007**, *72*, 7511–7522.

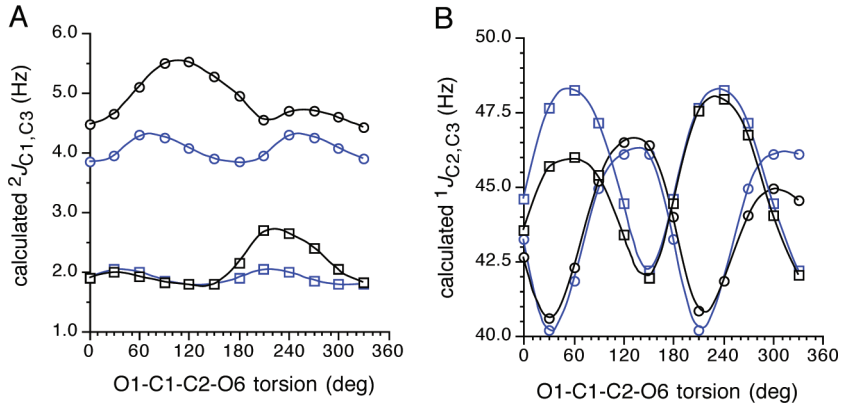

FIGURE 10. Effect of C1−C2 bond rotation on $^2J_{C1,C3}$ (A) and $^1J_{C2,C3}$ (B) in **7/8** (circles) and **9/10** (squares). Black symbols = protonated form; blue symbols = ionized form. Data taken from the FXS series.

SCHEME 4. Hyperconjugative Effects on $r_{C1,C2}$ and $^1J_{C1,C2}$ in the Ionized Form of 2α*p*

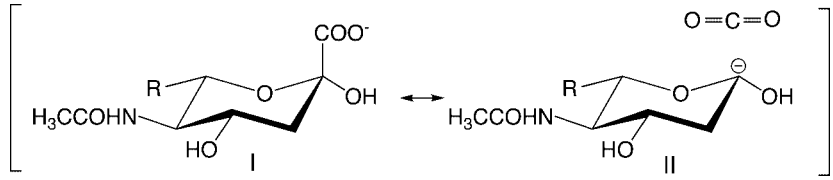

$^2J_{C2,C6}$ in **2** is analogous to $^2J_{C1,C5}$ in D-aldopyranosyl rings in the $^4C_1$ conformation, which depends on anomeric configuration (∼0 Hz in β-aldopyranoses, ∼−2 Hz in α-aldopyranoses).[27,28] The axial O2 in **2**β*p* mimics the axial O1 in α-D-aldohexopyranosyl rings ($^4C_1$) and elicits a comparable coupling, whereas the equatorial O2 in **2**α*p* mimics that in the corresponding β-aldopyranoses and little or no coupling is observed. DFT calculations (Figure 11B) show $^2J_{C2,C6}$ in **2**α*p* to be considerably more sensitive to C1−C2 bond rotation than **2**β*p*, mimicking behavior observed for $^2J_{C2,C4}$.

$^3J_{C2,C7}$ is large in **2**α*p* and **2**β*p* (3.1–3.6 Hz), consistent with a C2−O6−C6−C7 torsion angle of ∼180°. The coupling is slightly larger in **2**α*p*, presumably because of the terminal "in-plane" equatorial O2. Similar terminal substitution effects have been reported for analogous $^3J_{C1,C6}$ values in aldohexopyranosyl rings.[27,29] Ionization state affects this coupling minimally. DFT calculations (Figure 11C) show $^3J_{C2,C7}$ to be more sensitive to C1−C2 bond rotation in **2**α*p* than in **2**β*p*, a pattern also observed for $^2J_{C2,C4}$ and $^2J_{C2,C6}$.

$^1J_{C3,C4}$ is 35.8 Hz in **2**α*p* and **2**β*p* and shows no sensitivity to COOH ionization state. Of the three $^1J_{CC}$ measured in this study, $^1J_{C3,C4}$ is smallest, $^1J_{C1,C2}$ largest, and $^1J_{C2,C3}$ intermediate in magnitude. $^2J_{C3,C5}$ and $^{3+3}J_{C3,C6}$ are very small or zero in **2**α*p* and **2**β*p*. The disparity between experimental and calculated $^2J_{C3,C5}$ values (Table 6) probably stems from the effects of C4−O4 bond conformation on coupling magnitude. Coupling is expected to be enhanced when both O4 lone pairs are *anti* to the C3−C4 and C4−C5 bonds (*i.e.*, H4−C4−O4−H torsion angle of 180°; Scheme S2).

F. Conformation About the C6−C7 Bond. Prior studies have examined the preferred conformation of the exocyclic glycerol fragment of **2**. Czarniecki and Thornton[18,19] concluded that the favored C6−C7 bond conformation is that having H6 roughly *anti* to C8, a conformation presumably stabilized by two H-bonds between O6 (acceptor) and O8H, and between N5H and O7 (acceptor). In this conformation, H6 and H7 are approximately *gauche*, which is consistent with the small $^3J_{H6,H7}$ (1.2 Hz; Table 1). In contrast, Brown and co-workers[15] concluded, based on steric arguments, that of the two potential *gauche* O6−C6−C7−O7 conformations consistent with a small $^3J_{H6,H7}$, that having H6 approximately *anti* to O7 is preferred.

In the present work, an additional long-range ^{13}C−^{1}H coupling, $^4J_{C2,H7}$, was observed in **2**β*p* (Figure 1E; Table 3) that serves to distinguish between the two potential *gauche* O6−C6−C7−O7 conformations. Analogous $^4J_{COCCH}$ have been reported recently in D-galactopyranosyl rings ($^4J_{C1,H6S}$) and were shown to depend highly on geometry about the C1−O5−C5−C6−H6*R*/*S* fragment, with in-plane (W-shaped) arrangements leading to measureable couplings.[23] In this prior work, couplings as large as 1.1 Hz were observed in conformationally constrained compounds. Observation of a 0.8 Hz coupling between C2 and H7 in **2**β*p* supports the contention that the C6−C7 conformation orienting H6 approximately *anti* to O7 (coplanar C2−O6−C6−C7−H7 fragment) is highly populated in solution. If the very small value of $^3J_{H6,H7}$ is interpreted as support for a relatively rigid torsion angle of ∼−70° to −80°, then the magnitude of $^3J_{H6,H7}$ would be consistent with a geometry having H7 slightly out-of-plane, although we cannot dismiss a two-state exchange involving both H6−C6−C7−H7 *gauche* conformers, with one highly favored. Other *J*-couplings not measured in this work (e.g., $^3J_{C5,H7}$, $^3J_{C5,C8}$) might shed further light on this problem.

G. Comparison of J_{CC} in 2β*p*, 3-Deoxy-β-D-fructopyranose (11) and β-D-fructopyranose (12). The preferred chair conformations of 3-deoxy-β-D-fructopyranose (**11**), β-D-fructopyranose (**12**), and **2**β*p* are similar (i.e.,$^2C_5$), allowing useful comparisons of related couplings in these structures. $^1J_{C1,C2}$ is ∼22 Hz larger in **2**β*p* at pH 2.0 than in **11** and **12** (Table 7). In contrast, $^1J_{C2,C3}$ and $^1J_{C3,C4}$ are 4–6 Hz larger in **12** than in **2**β*p*, presumably due to the additional hydroxyl group

(28) King-Morris, M.; Serianni, A. S. *J. Am. Chem. Soc.* **1987**, *109*, 3501–3508.

(29) Bose, B.; Zhao, S.; Stenutz, R.; Cloran, F.; Bondo, P. B.; Bondo, G.; Hertz, B.; Carmichael, I.; Serianni, A. S. *J. Am. Chem. Soc.* **1998**, *120*, 11158–11173.

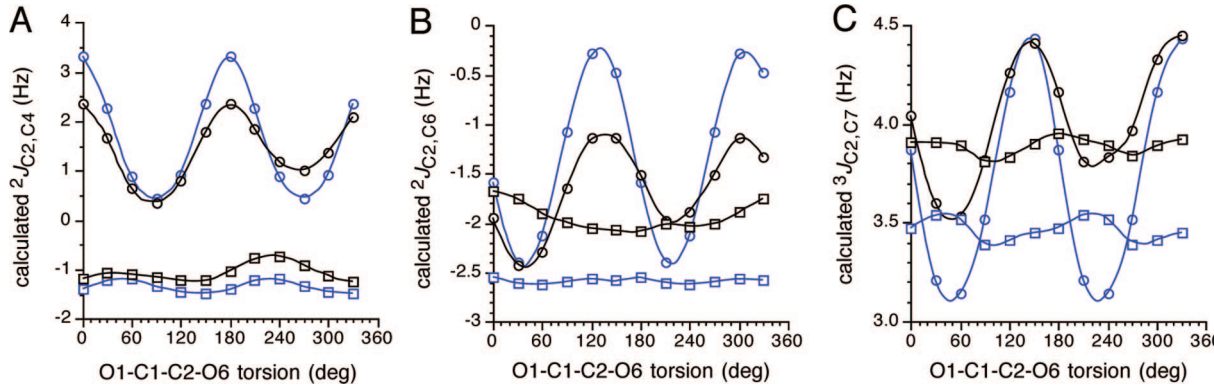

FIGURE 11. Effect of C1−C2 bond rotation on $^2J_{C2,C4}$ (A), $^2J_{C2,C6}$ (B), and $^3J_{C2,C7}$ (C) in **7/8** (circles) and **9/10** (squares). Black symbols = protonated form; blue symbols = ionized form. Data taken from the FXS series.

TABLE 8. Effect of Solvent on Calculated Spin-Couplings in 9 and 10[a]

	9			10		
J-coupling (Hz)	FX	FXS	expt	FX	FXS	expt
$^1J_{C1,C2}$	81.7	80.0	71.7	62.9	70.4	66.3
$^1J_{C2,C3}$	44.5	44.9	41.0	45.2	45.8	41.1
$^1J_{C3,C4}$	35.6	36.0	35.8	36.3	36.4	35.6
$^2J_{C1,C3}$	+2.0	+2.1	+1.7	+1.8	+1.9	+1.4
$^2J_{C2,C4}$	−1.1	−1.1	−1.5	−1.6	−1.4	−1.5
$^2J_{C2,C6}$	−2.1	−1.9	−1.9	−3.3	−2.6	−2.1
$^3J_{C1,C4}$	3.4	3.4	3.3	2.2	2.7	3.1
$^3J_{C1,C6}$	4.5	4.1	3.3	2.6	3.1	3.1
$^3J_{C2,C7}$	4.0	3.9	3.2	3.2	3.5	3.1
$^3J_{C1,H3ax}$	2.0	2.0	1.6	1.2	1.6	1.0
$^3J_{C1,H3eq}$	0.6	0.5	∼0	0.5	0.5	∼0
$^3J_{C2,H6}$	1.3	1.8	∼1.3	1.5	1.8	1.2
$^2J_{C2,H3ax}$	−2.8	−2.7	−3.6	−3.7	−3.0	−3.4
$^2J_{C2,H3eq}$	−2.9	−2.7	−3.9	−2.6	−2.5	−3.5
$^1J_{C3,H3ax}$	131.9	132.0	129.8	131.5	130.4	129.1
$^1J_{C3,H3eq}$	139.6	138.4	133.5	135.6	135.2	132.5
$^2J_{C3,H4}$	−1.9	−1.7	−2.1	−2.0	−1.7	−2.1
$^3J_{H3ax,H4}$	11.4	11.5	11.4	11.9	11.8	11.5
$^3J_{H3eq,H4}$	5.2	5.3	4.9	5.4	5.4	4.9
$^2J_{H3ax,H3eq}$	−12.7	−12.9	−13.1	−13.3	−13.1	−13.0
$^3J_{H4,H5}$	10.4	9.9	10.1	9.7	9.8	9.9
$^3J_{H5,H6}$	10.6	10.7	10.3	10.2	10.7	10.5

[a] Reported couplings were obtained by averaging the couplings calculated in the 12 C1−C2 rotamers of each structure. Experimental values are taken from this paper.

on C3 in the former.[30] $^2J_{C1,C3}$ is ± 3.4 Hz in **11** and ∼+1.7 Hz in **2**βp. $^3J_{C1,C4}$ and $^3J_{C1,C6}$ are larger in **2**βp than in **11** and **12**; since the dihedral angles are similar (∼180°), these differences are probably due mainly to different electronegative substituent effects at the terminal (C1) carbon. $^2J_{C2,C6}$ is very similar in **2**βp and **12**, but $^2J_{C2,C4}$ is smaller in **12** than in **2**βp. $^2J_{C3,C5}$ is small in **2**βp and **12**.

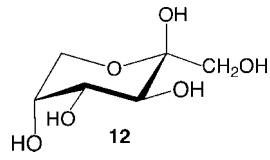

12

H. Effect of Solvation on Computed Couplings in 9 and 10. The effect of including solvent on calculated *J*-couplings in **9** and **10** is summarized in Table 8. Comparisons were made between calculated couplings obtained in the FX and FXS series. Inclusion of solvent caused relatively minor changes in calculated J_{HH}, J_{CH}, and J_{CC} values in the protonated form **9** (Δ 0.1–1.7 Hz for ^1J; Δ 0–0.6 Hz for ^2J and ^3J). In **10**, J_{HH} values were little affected by the inclusion of solvent, presumably because these pathways are relatively far removed from the site of ionization. In contrast, $^1J_{C1,C2}$ increases significantly (7.5 Hz) in the solvent calculations. The difference in $^1J_{C1,C2}$ between **9** and **10** is 18.8 Hz for *in vacuo* data and 9.6 Hz for solvated data, whereas the experimental difference is 5.5 Hz. It is noteworthy, however, that, in general, calculated $^1J_{CC}$ are not quantitative in any data set (they are often overestimated), whereas only minor changes are observed in longer range J_{CH} and J_{CC} when solvent is included in the calculations. When changes are observed in J_{CC} and J_{CH} values in **10** involving C1 and C2, the shift is more often to more positive values. These results suggest that inclusion of solvent in studies of calculated *J*-couplings in charged monosaccharides may be important to more closely mimic $^1J_{CC}$ values near the site of ionization, but effects on more remote couplings appear modest.

Conclusions

Many biologically important oligosaccharides attached to glycoproteins contain *N*-acetyl-neuraminic acid linked glycosidically as a terminal residue. The conformational properties of Neu5Ac-containing linkages in solution are poorly understood, largely because experimental parameters to assign these properties are limited in number. The present work was conducted to support anticipated studies of trans-glycoside *J*-couplings involving Neu5Ac since these parameters hold potential as NMR probes to investigate the solution behaviors of these linkages. In contrast to trans-glycoside *J*-couplings involving Glc, Gal, Fuc, and GlcNAc residues, *J*-couplings involving Neu5Ac are potentially subject to the effects of solution pH, since an ionizable COOH functionality is proximal to the glycosidic linkage. The present work aimed to evaluate the effect of this factor on intraresidue J_{HH}, J_{CH}, and J_{CC} as a means of predicting related effects on trans-glycoside J_{CH} and J_{CC}. New information on J_{CH} and J_{CC} involving C1, C2, and C3 of Neu5Ac was also obtained for coupling pathways having defined structure imposed by the pyranosyl ring. These "fixed pathway" couplings will provide a means to validate calculated trans-glycoside couplings since their pathways mimic those across the linkage and, importantly, are associated with constrained torsion angles.

Several important findings emerged from this work. $^1H-^1H$ *J*-couplings in **2**αp and **2**βp are largely independent of solution

(30) Duker, J.; Serianni, A. S. *Carbohydr. Res.* **1993**, *249*, 281–303.

pH, presumably because these coupling pathways are relatively remote from the site of ionization. DFT calculations in the presence of solvent reproduce intraring J_{HH} reasonably well.

Geminal J_{CH} involving C2 and $H3_{ax}/H3_{eq}$ are negative in sign and can be used to distinguish between Neu5Ac pyranose anomers in a manner similar to that reported previously for $^3J_{C1,H3ax/H3eq}$.[19a,b] The different magnitudes observed for the three *gauche* pathways for $^3J_{C1,H3ax/H3eq}$ in **2**α*p* and **2**β*p* do not appear to be caused by substituent effects but instead by differences in the endocyclic C−C−C−H torsion angles associated with these couplings.

$^1J_{C1,C2}$ values in **2** depend on pyranose anomeric configuration and on solution pH. This coupling is larger in the β-pyranose and decreases in both anomers with increasing pH. DFT calculations showed that the reduction in $^1J_{C1,C2}$ with increasing pH is accompanied by an increase in the C1−C2 bond length. The latter correlation can be explained by a hyperconjugative mechanism in which the C1−C2 bond is weakened in the ionized state.

Rotation of the C1−C2 bond exerts significant effects on $^1J_{CC}$, $^2J_{CC}$, and $^3J_{CC}$ values involving C2 of Neu5Ac. The extent of this effect depends on anomeric configuration for the latter two coupling types. Generally, these couplings are more sensitive to C1−C2 bond rotation in the α-pyranose for reasons that are presently unclear.

Recent studies of aldohexopyranosyl rings have shown that $^4J_{COCCH}$ involving C1 can be used as constraints to evaluate exocyclic CH_2OH conformation.[23] A related effect exists in Neu5Ac pyranosyl rings, where analogous coupling is observed between C2 and H7. This observation provides constraints on the C6−C7 bond torsion in **2**β*p* in solution, favoring a conformation having H6 approximately *anti* to O7.

DFT calculations of $^1J_{C1,C2}$ in **2** yielded values in closer agreement with the experimental couplings when solvent was included in the calculation. However, the effect of solvent on calculated geminal and vicinal couplings involving C1−C3 is small or negligible, such that at the present level of theory, no distinct advantage is gained by including solvent when longer-range couplings are the focus of attention. These findings have important implications for future studies of trans-glycoside *J*-couplings involving **2** and *J*-couplings in other ionizable sugars such as uronic acids.

A set of standard, experimental J_{CH} and J_{CC} values involving C1−C3 of **2** have been measured that mimic specific trans-glycoside *J*-couplings involving Neu5Ac residues. Intraresidue $^3J_{C1,C6}$ in **2**α*p* is related to $^3J_{C1,C3'}$in **5**, and the experimental value of $^3J_{C1,C6}$ is associated with a torsion angle of ∼−60°, providing a reference value in the construction of a $^3J_{C1,C3'}$ Karplus curve. Likewise, $^3J_{C2,C7}$ in **2**α*p* mimics trans-glycoside $^3J_{C2,C2'}$ and $^3J_{C2,C4'}$ in **5**, providing standard couplings for torsions of ∼180°. Based on the present findings, these couplings are expected to be relatively unaffected by the ionization state of the COOH group. On the other hand, the present results suggest that rotation about the C1−C2 of **2** may affect some J_{CH} and J_{CC} values significantly, and this factor, largely unappreciated prior to this work, will need to be considered in studies of trans-glycoside couplings. Present data suggest that conformational preferences about the C1−C2 bond of Neu5Ac anomers differ, that inclusion of solvent–water significantly reduces the activation barriers for C1−C2 bond rotation, and that activation barriers to C1−C2 bond rotation are higher for the carboxylate anion than for the protonated acid.

Acknowledgment. This work was supported by a grant from the National Institutes of Health (GM) (to A.S.). The Notre Dame Radiation Laboratory is supported by the Office of Basic Energy Sciences of the United States Department of Energy. This is Document No. NDRL-4743 from the Notre Dame Radiation Laboratory.

Supporting Information Available: Monomeric forms of **2** in aqueous solution (pH 2) (Scheme S1); initial geometries of **7**−**10** (Scheme S2); deuterium exchange of C3 protons of **2** in mild aqueous base (Scheme S3); preferred C1−C2 bond conformations in **2** (Scheme S4); projections for $^2J_{C2,H3ax}$ and $^2J_{C2,H3eq}$ in **2**α*p* and **2**β*p* (Scheme S5); table of ^{1}H chemical shifts of **2** at p^{2}H 2.0 and pH 8.0 (Table S1); table of ^{13}C chemical shifts of **2** at p^{2}H 2.0 and pH 8.0 (Table S2); figure showing amide signals of **2** at p^{2}H 2.0 and pH 8.0 (Figure S1); figure showing H5 signals of **2**β*p* at p^{2}H 2.0 and pH 8.0 (Figure S2); complete reference 10; and Cartesian coordinates for **7**−**10**. This material is available free of charge via the Internet at http://pubs.acs.org.

JO702204X